Biogeosciences Discuss., 6, 6249–6269, 2009
www.biogeosciences-discuss.net/6/6249/2009/

Biogeosciences Discussions

Biogeosciences Discussions is the access reviewed discussion forum of *Biogeosciences*

Coupling of surface pCO_2 and dissolved oxygen in the northern South China Sea: impacts of contrasting coastal processes

W. Zhai[1], **M. Dai**[1], **and W. Cai**[2]

[1]State Key Laboratory of Marine Environmental Science, Xiamen University, Xiamen 361005, China
[2]Departments of Marine Sciences, the University of Georgia, GA 30602-3636, USA

Received: 8 June 2009 – Accepted: 9 June 2009 – Published: 30 June 2009

Correspondence to: M. Dai (mdai@xmu.edu.cn)

Published by Copernicus Publications on behalf of the European Geosciences Union.

Abstract

We examined the relationship between CO_2 partial pressure (pCO_2) and dissolved oxygen (DO) based on a cruise conducted in July 2004 to the northern South China Sea, spanning from estuarine plume, coastal upwelling and deep basin areas. Distinct relationships between pCO_2 and DO saturation were identified in different regimes. In coastal upwelling areas and the Pearl River estuary, biological drawdown of pCO_2 and production of O_2 were simultaneously observed. The two properties were coupled with each other primarily via photosynthesis and respiration. The stoichiometric relationship of the two properties however, was quite different in these two environments due to different values of the Revelle factor. In the offshore areas, apart from the estuary and upwelling, the dynamics of pCO_2 and DO were mainly influenced by air-sea exchange during water mixing. Given the fact that air-sea re-equilibration of O_2 is much faster than that of CO_2, the observed pCO_2-DO relationship deviated from that of the theoretical prediction based on the Redfield relationship in the offshore areas.

1 Introduction

The production of organic carbon leads to drawdown of CO_2 partial pressure (pCO_2) and increases in dissolved oxygen (DO), while respiration/remineralization is associated with CO_2 release and DO consumption. It is therefore reasonable to expect a correlation between pCO_2 and DO in the surface ocean. Such a correlation has been shown to have implications for upper ocean metabolic status (DeGrandpre et al., 1997; 1998; Álvarez et al., 2002; Gago et al., 2003; Carrillo et al., 2004; Kuss et al., 2006; Körtzinger et al., 2008). Indeed, many studies have used simultaneous measurements of DO and CO_2 in seawater to investigate the effects of metabolic processes on the oceanic CO_2 dynamics (Borges and Frankignoulle, 2001; Guéguen and Tortell, 2008; Zhai and Dai, 2009). However, it should be pointed out that sea surface pCO_2 is buffered by the marine carbonate system, while DO is not associated with any buffer

BGD

6, 6249–6269, 2009

system. Therefore the relationship between the pCO_2 and DO variation in the euphotic zone may differ between different biogeochemical settings (DeGrandpre et al., 1997; 1998), thereby the different pCO_2-DO relationship may have different implications on metabolic status. The coastal system, due to its large gradient in physical-biogeochemistry may particularly be prone to such variability. Thus far, there have only been a few reports attempting to elucidate such relationships in the context of ecosystem metabolic balance based on high spatial-resolution measurements of CO_2 and O_2 (e.g. Carrillo et al., 2004).

In the summer of 2004, we conducted underway measurements of surface pCO_2 and DO in the northern South China Sea, spanning from estuarine plume, coastal upwelling and deep basin areas (Fig. 1). This unique dataset allowed for a close examination of how different relationship between pCO_2 and DO would be in different regimes such as open regions and coastal areas influenced by either estuarine plume and/or coastal upwelling, and how these differences would imply for metabolic status.

2 Materials and methods

2.1 Study area and survey transects

The South China Sea (SCS) is the world largest marginal sea located at low latitudes in the tropic and subtropical region. While its maximum depth exceeds 5000 m, it has extensive shelf system in the northwestern and southern boundaries with a mean depth of only 1350 m (Wong et al., 2007). The northern shelf and slope (i.e. the northern SCS, ~200 km broad) is oligotrophic, low-productive (Wong et al., 2007; Chen and Chen, 2006) and serve as a net source of atmospheric CO_2 especially in summer (Zhai et al., 2005a). This is in contrast to many significant CO_2 sink cases in middle-latitude continental shelf systems (Cai and Dai, 2004; Borges et al., 2005; Cai et al., 2006).

The nearshore waters of the northern SCS are quite different from the oligotrophic

offshore regions. Fed by the Pearl River, a world major river located in southern China, the productive estuarine plume may extend southeastward to up to a few hundreds of kilometers off the estuary mouth in flooding seasons (Dai et al., 2008; Gan et al., 2009). In addition to the estuarine plume, the northern SCS is also influenced by seasonal upwelling along the Chinese coast (Fig. 1; Han, 1998; Wu and Li, 2003; Gan et al., 2009; Jing et al., 2009). Both processes peak in summer as a result of the prevailing rain-bearing southwest monsoon from late May to September (Han, 1998), and both contribute a significant amount of new nutrients to the coastal waters, inducing dramatic changes of surface pCO_2 and DO through enhanced primary productivity (e.g. Dai et al., 2008). The chl-*a* dataset clearly shows the contrast between productive nearshore and oligotrophic offshore areas in the northern SCS (Fig. 1; Huang et al., 2008).

Our cruise was conducted on 6–23 July 2004 on board the R/V Yanping II. During this cruise, we performed underway measurements of temperature, salinity, DO and pCO_2 along four shelf-crossing transects (Fig. 1, sequentially marked as B, D, C and A from the cruise beginning to the end) and an alongshore transect (E). Transect A covers the Pearl River estuary (114°00′ E 22°00′ N, PRE hereafter) to the southwest to the Dongsha Islands (115°48′ E 20°10′ N). Finally, ending with the transect between station B1 (116°54′ E 20°52′ N) and the deep basin station (Station S1 @ 116°00′ E 18°00′ N) is named Transect S (Fig. 1). In this study, 70-m isobath was used to classify nearshore areas or coastal waters from the deeper offshore region.

2.2 Sampling, analyses and data processing

During the cruise, surface water (at a depth of 1–2 m) was continuously pumped from a side intake using an underway pumping system similar to that previously described in Zhai et al. (2005b). Sea surface temperature (SST) and salinity were measured continuously using a SEACAT thermosalinograph system (CTD, SBE21, Sea-Bird Co.) with an in situ temperature sensor. Data were recorded every 6 s and averaged to 1 min. This underway CTD system was calibrated just prior to the cruise.

Surface water pCO_2 was determined using an underway system with a continuous flow and cylinder-type equilibrator (9 cm in diameter and 20 cm long) that is filled with plastic balls and enclosed with ~100 mL of the headspace (Zhai *et al.*, 2005b). During this cruise, the equilibrator was exposed to the outdoor open air on deck. A Yellow Springs Instrument meter (YSI®6600) was used to continuously measure temperature in the equilibrator. Based on inter-calibration testing, we estimated that all onboard temperature sensors are consistent with each other within 0.1°C. After the equilibrator and dehydration, the CO_2 mole fraction in dry air (xCO_2) was detected continuously using a Li-Cor® NDIR spectrometer (Li-7000). Data were recorded every 5 s and averaged to 1 min. The NDIR spectrometer was calibrated regularly against 4 CO_2 gas standards. xCO_2 of the standards ranged from 138 to 967 µmol mol^{-1}. pCO_2 was converted from corrected xCO_2 based on barometric pressure around the Li-7000 detector or air pressure along the transect. The latter were collected every minute with an onboard weather station at 10 m height above the sea surface. Comparison between the two air pressure datasets revealed consistency at a relative error level of ~0.1% (i.e. ~1 hPa). The Weiss & Price (1980) saturated water vapor pressure and the Takahashi et al. (1993) temperature effect coefficient of 4.23% °C^{-1} were used to calculate the in situ pCO_2. The temperature difference between the equilibrator and the sea surface was 0.21–0.29°C. The overall uncertainty of the xCO_2 measurements and pCO_2 data processing is <1% as constrained by our standard gases (Zhai et al., 2005a; 2005b).

Air pCO_2 was determined in the first 5 d, every 1–3 h in daytime and every 4 h in nighttime, using the same NDIR spectrometer and dehydration system. The bow intake from which atmospheric air was pumped was installed at ~6 m above the water surface to avoid contamination from the ship. The air pCO_2 data were corrected to 100% humidity at SST and sea surface salinity.

Surface DO was continuously measured using a pulsed polarographic electrode incorporated with the above-mentioned YSI meter. Data were recorded every 12 s and averaged to 1 min. The DO sensor was pre-calibrated against air saturated pure water and post-calibrated by simultaneous discrete Winkler DO data. These discrete sam-

ples were either collected via a side vent of our pumping system or obtained using 2.5-L Go-Flo bottles during general station work. DO concentration at equilibrium with the atmosphere was calculated from the Benson and Krause (1984) equation and local air pressure.

According to Broecker and Peng (1982) and Stigebrandt (1991), we used the 2.5% super-saturation as the effective DO saturation level considering the bubble effect. We also define excess oxygen (ExcessO_2 hereafter) as Eq. (1) to reflect evasion or invasion of atmospheric O_2:

$$\text{Excess}O_2 = [O_2] - 1.025 \times [O_2]_{eq} \quad (1)$$

where $[O_2]$ is the field-measured DO concentration; $[O_2]_{eq}$ is the DO concentration at equilibrium with the atmosphere, calculated from the Benson and Krause (1984) equation and local air pressure. The negative excess O_2 suggests an O_2 deficit while a positive value means O_2 emission from water to the atmosphere.

3 Results

3.1 Data overview

During the cruise, two high salinity water masses were identified (Figs. 2, 3). One was a typical SCS surface water with salinity ~33.7–34.5 and SST ~28–31°C. All of the offshore areas of the four cross-shelf transects and the eastern area of transect E are dominated by this water mass (Fig. 2). In this water mass, surface DO was slightly oversaturated (102%–110%), while pCO_2 ranged 370–400 µatm. This is consistent with the generally oligotrophic and low productive feature of the SCS surface water (Zhai et al., 2005a; Chen and Chen, 2006; Tseng et al., 2007).

Another high salinity water mass was characterized by low temperatures of 25.5–26.5°C (Figs. 2, 3), suggesting the influence of subsurface water upwelling. This water mass was limited to the nearshore area of Transect B and to the west side of Transect E.

The nearshore area of Transect D was also influenced by the same low temperature water as observed in Transect E (Fig. 2). These two upwelling influenced coastal areas have been well defined by both field measurements (Wu and Li, 2003) and numerical modeling (Jing et al., 2009). The upwelling may support higher productivity due to new nutrient input from the depth. Thus, moderate to high chl-*a* levels were observed in those upwelling influenced areas, especially in the nearshore areas of Transect B (Fig. 1; Huang et al., 2008). Significantly oversaturated DO data of 120%–138% associated low temperature were also observed in those upwelling-influenced areas (Fig. 2). However, in the upwelling-influenced areas, pCO_2 varied in a large range between 280 and 440 µatm (Fig. 2), of which the highest pCO_2 of >400 µatm was observed at the west side of Transect E (Fig. 2e).

The low salinity water (S<33) can also be clustered into two groups (Fig. 3). One has a similar temperature (~28.5°C) to the PRE water (27–28°C, Fig. 2a), situated in nearshore areas of Transects A, B, C and E (Fig. 2). Another significant low-salinity water mass had fairly high temperature (30.5–31.0°C) which is located in offshore water of Transect B (Fig. 2b). The latter water mass had relatively low chl-*a* (Fig. 1) and DO saturation (Fig. 2b) as compared to the upwelling influenced nearshore area. This offshore low-salinity water is likely an estuarine plume originated from the PRE, which is typical in this region in summer as reported by Gan et al. (2009). In fact, both May and July were major rainy months in 2004 within the drainage basin of the Pearl River. There an episodic and large-scale heavy rain of 100–300 mm occurred during 10–12 May 2004 (China MWR-BH, 2005). Therefore, the patchy offshore low-salinity water in Transect B may have originated from the PRE after this heavy rain induced flood and had mixed partially with typical northern SCS surface water.

Both of the two low-salinity water masses had relatively low pCO_2 of 310–350 µatm (Fig. 2), while DO varied from slightly over-saturated level of 103%–110% to highly over-saturated level of ~130% (Fig. 2b). Note that in the PRE and the adjacent coastal waters, salinity was <25 and surface DO saturation was no higher than 115% (Fig. 2a), although chl-*a* was as high as 3–5 µg L^{-1} (Fig. 1; Huang et al., 2008).

3.2 Relationship between pCO_2 and DO

In the PRE and nearshore region of Transect A, pCO_2 and DO saturation had a significant negative correlation (Fig. 4a). Based on our previous studies, the freshwater end of the PRE is characterized by high pCO_2 and low DO (Zhai et al., 2005b), while the seawater end has a significant pCO_2 drawdown and oversaturated DO due to strong algae blooms supported by high nutrients from the river (Dai et al., 2008). Fig. 4a generally reflected a combination of metabolic and physical processes in the PRE (see Sect. 4).

In the nearshore area of Transect B, pCO_2 and DO saturation had a significant negative correlation (Fig. 4b, slope=−164 µatm, r=−0.88), where a coastal upwelling system was associated (Figs. 1, 2b). This slope was translatable into the nearshore regions of Transect D and west side of Transect E (close to the Transect D) (Fig. 4d), where another upwelling system was also located (Figs. 1, 2e). In contrast, the offshore area of Transect B, pCO_2 and DO saturation distinctly followed another negative correlation (slope=−1465 µatm, r=−0.94, Fig. 4b) where an estuarine plume existed. In the offshore areas of Transects A, C and D, no correlation can be developed between pCO_2 and DO saturation (Fig. 4).

In summary, we observed three pCO_2-DO relationships, which implies different biogeochemical processes in different regimes of the northern SCS. Below we will discuss them in details.

4 Discussion

4.1 Linking DO to pCO_2 in the upwelling induced bloom areas based on Redfield ratio and Revelle factor

In the bloom areas, metabolic processes typically cause negatively correlated variations of dissolved inorganic carbon (DIC) and DO. However the relationship between

pCO_2 and DO is more complicated because pCO_2 is buffered by the marine carbonate system characterized by the Revelle factor. In contrast DO is not associated with any buffer system. The Revelle factor is defined as the ratio of fractional change in seawater pCO_2 to the fractional change in total DIC after re-equilibration, i.e. $\{[\partial pCO_2/pCO_2]/[\partial DIC/DIC]\}$ at a given temperature, salinity and alkalinity (Revelle and Suess, 1957; Sundquist et al., 1979). In the oligotrophic basin area of the northern SCS, the surface-water Revelle factor has been estimated to be about 9 (Tseng et al., 2007). Air-equilibrated surface DIC (1900 $\mu mol\,kg^{-1}$) in the offshore regions is taken from Tseng et al. (2007). The air-equilibrated pCO_2 is taken from the mean value of field measured atmospheric pCO_2.

In the following discussion, we converted the $ExcessO_2$ value into DIC change based on the classic Redfield Ratio. Then we used the Revelle factor to convert DIC change induced by $ExcessO_2$ into pCO_2 change at the given temperature, thereby linking $ExcessO_2$ to pCO_2 change in order to characterize the metabolic processes. In light of the effects of heating/cooling on both the pCO_2 and DO saturation (4.23% $^{\circ}C^{-1}$ vs. 1.60% $^{\circ}C^{-1}$), we normalized sea surface pCO_2 to the mean SST (29°C) following the approach of Zhai et al. (2005a) to examine the relationship between the temperature normalized pCO_2 ($NpCO_2$ hereafter) and $ExcessO_2$. Therefore, several possible photosynthesis-respiration-dominative lines of $NpCO_2$ vs. $ExcessO_2$ at different Revelle factors of 9 and 11 were plotted in Fig. 5a according to Eq. (2):

$$\begin{aligned}\delta NpCO_2 &= RF \times (NpCO_2^0/DIC^0) \times \delta DIC \\ &= RF \times (NpCO_2^0/DIC^0) \times (-\delta ExcessO_2) \times (106/138) \qquad (2)\end{aligned}$$

where prefix δ means a differential change, superscript 0 the air-equilibrated value, RF the Revelle factor, 106/138 the classic Redfield ratio between carbon and O_2 changes.

Both the datasets from the two coastal upwelling systems (nearshore areas of Transects B and D, together with west part of the Transect E) followed the seawater Redfield lines (Fig. 5a), although some $NpCO_2$ data were higher than the air-equilibrated level in the central areas of the two upwelling systems. This suggests that both pCO_2 and

BGD
6, 6249–6269, 2009

DO are mainly driven by biological photosynthesis and respiration in the upwelling-influenced nearshore regions except in the upwelling center where deep water of high pCO_2 was still observable. Another piece of evidence pointing to the fact that metabolic processes dominated the upwelling-influenced nearshore region is derived from higher surface chl-*a* concentrations (Fig. 1; Huang et al., 2008). Most significantly, high chl-*a* values of $>2\,\mu g\,L^{-1}$ were observed at two stations in and around the coastal area of Transect B (Fig. 1).

4.2 Influence of air-sea exchange on pCO_2-DO relationship in offshore regions

Away from the upwelling-influenced regions, however, the relationship of NpCO_2-ExcessO_2 was much different from what was shown in Fig. 5a. In the offshore estuarine plume area of Transect B, although NpCO_2 was still significantly correlated with ExcessO_2 (Fig. 5b), the slope was much higher than in those upwelling influenced nearshore waters. This suggests that such a relationship was not mainly derived from on site biological activity, rather it is modulated by a combination of metabolic and physical processes during the long-distance mixing with offshore waters.

It is important to point out that air-sea re-equilibration of CO_2 is slower than DO due to the chemical buffering capacity of the marine carbonate system (DeGrandpre et al., 1997; 1998). Therefore, we cannot directly predict DIC change during the long-distance transportation and mixing from O_2 change.

Based on the classic stagnant film model, the flux of gases between the atmosphere and water can be estimated by an empirical boundary-layer model for gas exchange: Flux=$D_{gas}/z \times \Delta C_{gas}$, where D_{gas} is the molecular diffusion coefficient, z the empirical thickness of a hypothetical stagnant boundary layer, ΔC_{gas} the concentration deficit or overstock in water surface. Thus an empirical gas exchange ratio (ER) of ΔC_{O_2} (i.e. ExcessO_2) to ΔC_{CO_2} (free CO_2 deficit, $\Delta[CO_2^*]$ hereafter, estimated from air-sea pCO_2 difference at SST and Henry's law constant of CO_2) must be established first.

At the lowest seawater pCO_2 site in the offshore area of Transect B, $\Delta[CO_2^*]$

can be estimated as 1.18 µmol kg^{-1} based on air pCO_2~358 µatm and seawater pCO_2~313 µatm at SST ~30.7°C and salinity ~31.7 (Fig. 2b), while ExcessO_2 was observed as 12 µmol kg^{-1} (Fig. 5b). Therefore the ratio of ExcessO_2 to $\Delta[CO_2^*]$ was estimated as 10.7. This was nearly the lowest disequilibrium ratio in this region, which was apparently derived from chemical buffering effect of CO_2 during metabolic processes. Based on our field-measured dataset in this region, the ratio of ExcessO_2 to $\Delta[CO_2^*]$ varied between 9.7 and 22. This ratio, further based on the diffusion coefficient ratio of O_2 to CO_2 (~1.2, Broecker and Peng 1982), would lead to the lowest air-water exchange ratio of O_2 to CO_2~(9.7×1.2):1=12:1 in the offshore area of our Transect B, while the highest ratio ~(22×1.2):1=26:1.

Similar to Eq. (2), Eq. (3) gives the quantitative expression of NpCO_2 vs. DO at a given ER of O_2 to DIC:

$$\delta \mathrm{N}pCO_2 = \mathrm{RF} \times (\mathrm{N}pCO_2^0/\mathrm{DIC}^0) \times \delta\mathrm{DIC}$$
$$= \mathrm{RF} \times (\mathrm{N}pCO_2^0/\mathrm{DIC}^0) \times (-\delta\mathrm{Excess}O_2) \times (1/\mathrm{ER}) \quad (3)$$

Based on the above ER factors and Eq. (3), assuming a RF of 10, we can estimate the highest air-sea exchange induced slope of NpCO_2-ExcessO_2 plot in the offshore area of Transect B by $\delta \mathrm{N}pCO_2/\delta\mathrm{Excess}O_2 = -\mathrm{RF}\times(\mathrm{N}pCO_2^0/\mathrm{DIC}^0)\times(1/\mathrm{ER}) = -10\times(360/1900)\times(1/12) = \sim -0.15$ µatm-pCO_2 (µmol O_2 $kg^{-1})^{-1}$, or ~−35 µatm for the slope of pCO_2-DO% plot, given the saturated DO value ~220 µmol O_2 kg^{-1} in summer in the northern SCS. This suggests that an integration of the on-site metabolic processes prior to our cruise and the air-sea exchange during later buoyant transportation may have resulted in the unique pattern of the pCO_2-DO relationship in offshore region of our Transect B (see arrows in Figs. 4, 5b for reference). The relatively homogeneous but lower chl-*a* concentration in this region compared with the high values in nearshore area of our Transect A (Fig. 1, which is suggested as the source area of the offshore low-salinity region of Transect B) supported such a pattern. Similar patterns have been observed in the outer Changjiang (Yangtze River) Estuary, East China Sea (Zhai and Dai, 2009).

BGD
6, 6249–6269, 2009

In most offshore areas other than the estuarine plume area of Transect B, however, the NpCO_2/pCO_2 varied independently from ExcessO_2/DO (Figs. 4, 5b). This low metabolic signal between pCO_2 and DO in the offshore waters is consistent with the low chl-*a* (Fig. 1; Huang et al., 2008) and thereby represents the low regional productivity. Just prior to our cruise, both primary and new production was measured in our studied offshore region. Primary production (PP) was 31±12 mmol C m^{-2} d^{-1} in the basin and 72±22 mmol C m^{-2} d^{-1} on the shelf (Chen and Chen, 2006). Both are among the lowest of the world's oceans. If we use the average photosynthetic rate in 100 m euphotic water column, at a diurnal time scale, overall impact of biological activity on surface CO_2 system may be no more than 0.8 µmol C L^{-1} (<1.5 µatm the pCO_2, converted from Revelle factor 9 as discussed above) and DO<1.0 µmol L^{-1} (~0.5% the saturated DO). Both are insignificant relative to field measured air-sea difference values of pCO_2 and DO. Moreover, the new production was determined to be only ~7% (shelf) to 30% (basin) of the PP, indicating that the PP was mostly recycled on a daily time scale (Chen and Chen, 2006). Therefore, the net effects of biological activity on both pCO_2 and DO were minor in the outer shelf/slope and basin waters.

4.3 Influence of weak CO_2 buffer system in PRE and adjacent nearshore areas

In the PRE, however, DIC was ~1500 µmol kg^{-1} (Dai et al., 2008) and the Revelle factor varied from ~19@S~15 to ~12@S~25 based on the conservative mixing line of carbonate system as summarized in Dai et al. (2008). This is apparently caused by higher concentrations of free CO_2 in the estuarine waters than in the offshore water (Zhai et al., 2005a; 2005b).

Thus we can model possible photosynthesis-respiration-dominative lines of NpCO_2 vs. ExcessO_2 in the PRE based on the classic Redfield ratio and possible Revelle factor of 12–19 (Fig. 5c). The reasonable agreement between data and predicted values (Fig. 5c) suggests that the drawdown of pCO_2 and enhancement of DO in the PRE are mainly influenced by on site primary production, while air-water gas exchange may

also have contributions, with much smaller effects than the offshore estuarine plume area apparently due to the shorter residence time over there.

The comparison of different NpCO_2-ExcessO_2 relationships between coastal upwelling influenced areas and the PRE (Figs. 5a,c) shows the significant effect of Revelle factor on surface pCO_2 dynamics. Although pCO_2-DO relationships in nearshore areas of Transects A and B were both dominated by the photosynthesis/respiration, the different Revelle factors resulted in different pCO_2-DO slopes in the two waters (Figs. 4a,b).

5 Conclusions

In this study, we have elucidated the effect of photosynthesis/respiration and air-water exchange on the changes in the coupling of pCO_2 and DO in a spectrum of coastal settings in the northern SCS. In the coastal upwelling influenced areas, both properties were mainly controlled by on site community metabolic processes. In the estuarine plume influenced regions, the pCO_2-DO relationship was controlled by the integrated effect of previous community metabolic processes and subsequent air-water exchange. Moreover, the chemical buffering of carbonate system also had significant effect on the relationship. Our data set has, for the first time, identified different influencing processes in contrasting systems based on field-measured data in a single study.

This study reveals that a combination of high-resolution CO_2 and O_2 measurements may provide valuable information of metabolic status in marine ecosystems. Yet the relationship generated therein may have different implications. This study exemplified a simple procedure to evaluate the community metabolic status based on surface pCO_2 and DO measurements, which may have applicability in many coastal systems with large gradient of changes in physical and biogeochemical settings.

Acknowledgement. This research was supported by the Natural Science Foundation of China through grants #90711005, #40731160624, #40876040 and #40821063. The manuscript preparation was supported by Key Laboratory of Marine Ecosystem and Biogeochemistry,

SOA, China through open fund #LMEB200802 and by internal fund of State Key Laboratory of Marine Environmental Science (Xiamen University) (#MELRI0701). We thank W. Ruan and F. Zhang along with the crew of R/V Yanping II for their much help during the sampling cruise, B. Chen and Z. Chen for their assistance in the data collection and J. Hartmann for his assistance with English.

References

Álvarez, M., Ríos, A. F., and Rosón, G.: Spatio-temporal variability of air-sea fluxes of carbon dioxide and oxygen in the Bransfield and Gerlache Straits during austral summer 1995–96, Deep-Sea Res. II, 49, 643–662, 2002.

Benson, B. B. and Krause, D.: The concentration and isotopic fractionation of oxygen dissolved in fresh water and seawater in equilibrium with the atmosphere, Limnol. Oceanogr., 29, 620–632, 1984.

Borges, A. V., Delille, B., and Frankignoulle, M.: Budgeting sinks and sources of CO_2 in the coastal ocean: Diversity of ecosystems counts, Geophys. Res. Lett., 32, L14601, doi:10.1029/2005GL023053, 2005.

Borges, A. V. and Frankignoulle, M.: Short-term variations of the partial pressure of CO_2 in surface waters of the Galician upwelling system, Prog. Oceanogr., 51, 283–302, 2001.

Broecker, W. S. and Peng, T. H.: Tracers in the Sea, Eldigio Press, Palisades, New York, 690 pp., 1982.

Carrillo, C. J., Smith, R. C., and Karl, D. M.: Processes regulating oxygen and carbon dioxide in surface waters west of the Antarctic Peninsula, Mar. Chem., 84, 161–179, 2004.

Cai, W.-J., Dai, M. H., and Wang, Y. C.: Air-sea exchange of carbon dioxide in ocean margins: a province-based synthesis, Geophys. Res. Lett., 33, L12603, doi:10.1029/2006GL026219, 2006.

Cai, W.-J. and Dai, M. H.: Comment on "Enhanced open ocean storage of CO_2 from shelf sea pumping", Science, 306, p. 1477, 2004.

Chen, Y.-L.L. and Chen, H.-Y.: Seasonal dynamics of primary and new production in the northern South China Sea: the significance of river discharge and nutrient advection, Deep-Sea Res. I, 53, 971–986, 2006.

China MWR-BH (Bureau of Hydrology, Ministry of Water Resources, China): Hydrological In-

formation Annual Report 2004, China Water Power Press, Beijing, China, 104 pp., 2005 (in Chinese).
Dai, M. H., Zhai, W. D., Cai, W. J., Callahan, J., Huang, B. Q., Shang, S. L., Huang, T., Li, X. L., Lu, Z. M., Chen, W. F., and Chen, Z. Z.: Effects of an estuarine plume-associated bloom on the carbonate system in the lower reaches of the Pearl River estuary and the coastal zone of the northern South China Sea, Cont. Shelf Res., 28, 1416–1423, 2008.
DeGrandpre, M. D., Hammar, T. R., and Wirick, C. D.: Short-term pCO_2 and O_2 dynamics in California coastal waters, Deep-Sea Res. II, 45, 1557–1575, 1998.
DeGrandpre, M. D., Hammar, T. R., Wallace, D. W. R., and Wirick, C. D.: Simultaneous mooring-based measurements of seawater CO_2 and O_2 off Cape Hatteras, North Carolina, Limnol. Oceanogr., 42, 21–28, 1997.
Guéguen, C. and Tortell, P. D.: High-resolution measurement of Southern Ocean CO_2 and O_2/Ar by membrane inlet mass spectrometry, Mar. Chem., 108, 184–194, 2008.
Gago, J., Gilcoto, M., Pérez, F. F., and Ríos, A. F.: Short-term variability of fCO_2 in seawater and air-sea CO_2 fluxes in a coastal upwelling system (Ría de Vigo, NW Spain), Mar. Chem., 80, 247–264, 2003.
Gan, J. P., Li, L., Wang, D. X., and Guo, X. G.: Interaction of a river plume with coastal upwelling in the northern South China Sea, Cont. Shelf Res., 29, 728–740, 2009.
Han, W. Y.: Marine chemistry in the South China Sea, Science Press, Beijing, China, 289 pp., 1998 (in Chinese).
Huang, B. Q., Lan, W. L., Cao, Z. R., Dai, M. H., Huang, L. F., Jiao, N. Z., and Hong, H. S.: Spatial and temporal distribution of nanoflagellates in the northern South China Sea, Hydrobiologia, 605, 143–157, 2008.
Jing, Z. Y., Qi, Y. Q., Hua, Z. L., and Zhang, H.: Numerical study on the summer upwelling system in the northern continental shelf of the South China Sea, Cont. Shelf Res., 29, 467–478, 2009.
Körtzinger, A., Send, U., Wallace, D. W. R., Karstensen, J., and DeGrandpre, M.: Seasonal cycle of O_2 and pCO_2 in the central Labrador Sea: Atmospheric, biological, and physical implications, Global Biogeochem. Cy., 22, GB1014, doi:10.1029/2007GB003029, 2008.
Kuss, J., Roeder, W., Wlost, K.-P., and DeGrandpre, M. D.: Time-series of surface water CO_2 and oxygen measurements on a platform in the central Arkona Sea (Baltic Sea): seasonality of uptake and release, Mar. Chem., 101, 220–232, 2006.
Revelle, R. and Suess, H. E.: Carbon dioxide exchange between atmosphere and ocean and

the question of an increase of atmospheric CO_2 during the past decades, Tellus, 9, 18–27, 1957.
Stigebrandt, A.: Computations of oxygen fluxes through the sea surface and the net production of organic matter with application to the Baltic and adjacent seas, Limnol. Oceanogr., 36, 444–454, 1991.
Takahashi, T., Olafsson, J., Goddard, J. G., Chipman, D. W., and Sutherland, S. C.: Seasonal variation of CO_2 and nutrients in the high-latitude surface ocean: a comparative study, Global Biogeochem. Cy., 7, 843–878, 1993.
Tseng, C. M., Wong, G. T. F., Chou, W. C., Lee, B. S., Sheu, D. D., and Liu, K. K.: Temporal variations in the carbonate system in the upper layer at the SEATS station, Deep-Sea Res. II, 54, 1448–1468, 2007.
Sundquist, E. T., Plummer, L. N., and Wigley, T. M. L.: Carbon dioxide in the ocean surface: the homogenous buffer factor, Science, 204, 1203–1205, 1979.
Weiss, R. F. and Price, R. A.: Nitrous oxide solubility in water and seawater, Mar. Chem., 8, 347–359, 1980.
Wong, G. T. F., Ku, T.-L., Mulholland, M., Tseng, C.-M., and Wang, D.-P.: The SouthEast Asian Time-series Study (SEATS) and the biogeochemistry of the South China Sea: an overview, Deep-Sea Res. II, 54, 1434–1447, 2007.
Wu, R. S. and Li, L.: A summary of studies on upwelling system in the South China Sea, J. Oceanogr. Taiwan Str., 22, 269–277, 2003 (in Chinese).
Zhai, W. D. and Dai, M. H.: On the seasonal variation of air-sea CO_2 fluxes in the outer Changjiang (Yangtze River) Estuary, East China Sea, Mar. Chem., doi:10.1016/j.marchem.2009.02.008, in press, 2009.
Zhai, W.D, Dai, M. H., Cai, W.-J., Wang, Y. C., and Hong, H. S.: The partial pressure of carbon dioxide and air-sea fluxes in the northern South China Sea in spring, summer and autumn, Mar. Chem., 96, 87–97, 2005a. [Erratum: Mar. Chem., 103, 209, 2007].
Zhai, W. D., Dai, M. H., Cai, W.-J., Wang, Y. C., and Wang, Z. H.: High partial pressure of CO_2 and its maintaining mechanism in a subtropical estuary: the Pearl River estuary, China, Mar. Chem., 93, 21–32, 2005b.

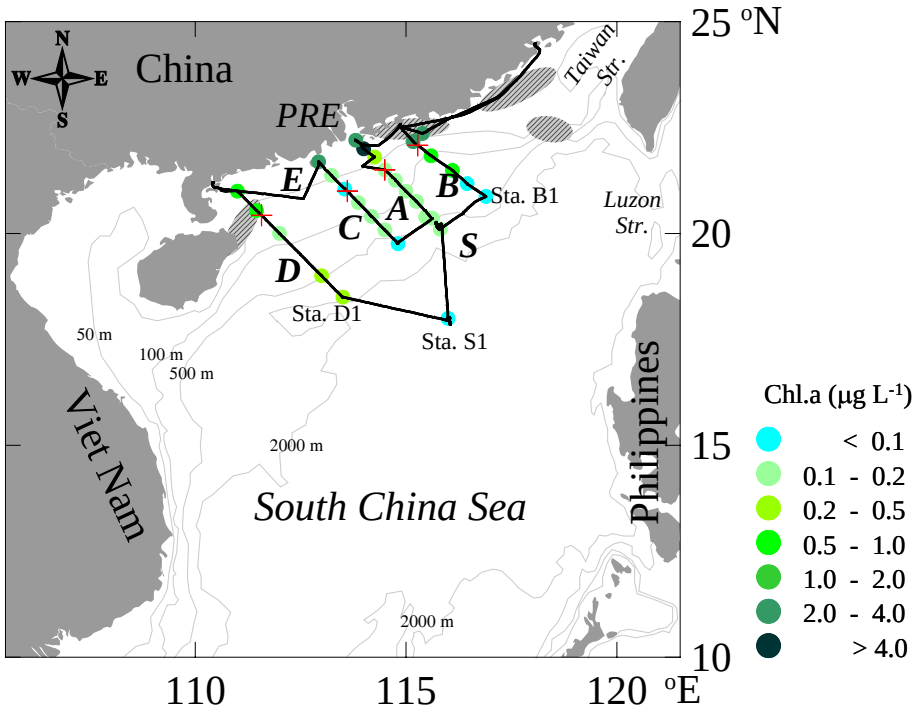

Fig. 1. Map of the northern South China Sea showing the cruise track and surveying transects (A, B, C, D, E and S). "+" symbols designate locations where we used to divide the shelf into nearshore and offshore areas in this study. Stations B1, D1 and S1 are also shown. Shadowed ellipses sketch typical summer upwelling locations based on Wu and Li (2003) and Jing et al. (2009). Discretely sampling data of surface chl-*a* concentrations were from Huang et al. (2008).

BGD
6, 6249–6269, 2009

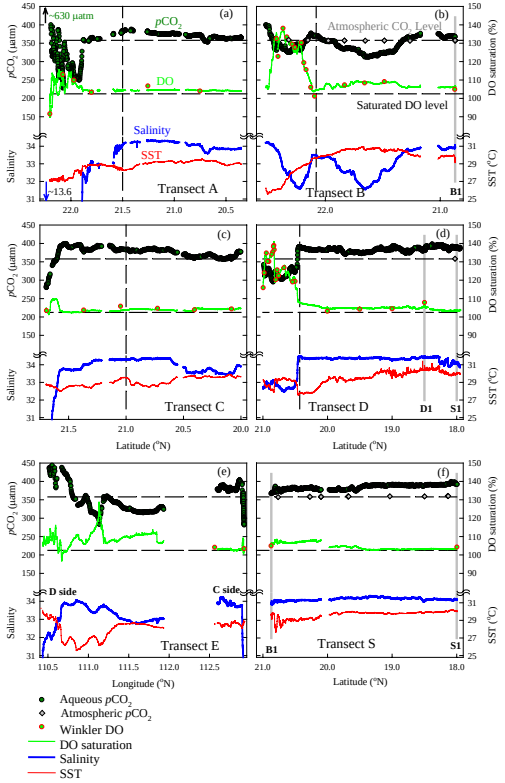

Fig. 2. Distribution of surface T, S, pCO_2 and DO along surveying transects. Note that Panels **(a–d)** and **(f)** are presented from the coast (north) to the deep basin (south). Panel **(e)** is presented from Transect D side (west) to Transect C side (east). A high pCO_2 of ~630 µatm and a low salinity of ~13.6 in the Pearl River estuary, as extended from Transect A were also marked in panel **(a)**. The vertical dashed lines in panels **(a–d)** show the locations with bathymetric depth of ~70 m, referring to Fig. 1. The vertical grey solid lines in panels **(b)**, **(d)** and **(f)** show Stations B1, S1 and D1, referring to Fig. 1. The horizontal dashed lines in each panel show atmospheric CO_2 level (upper) and saturated DO level (lower).

BGD
6, 6249–6269, 2009

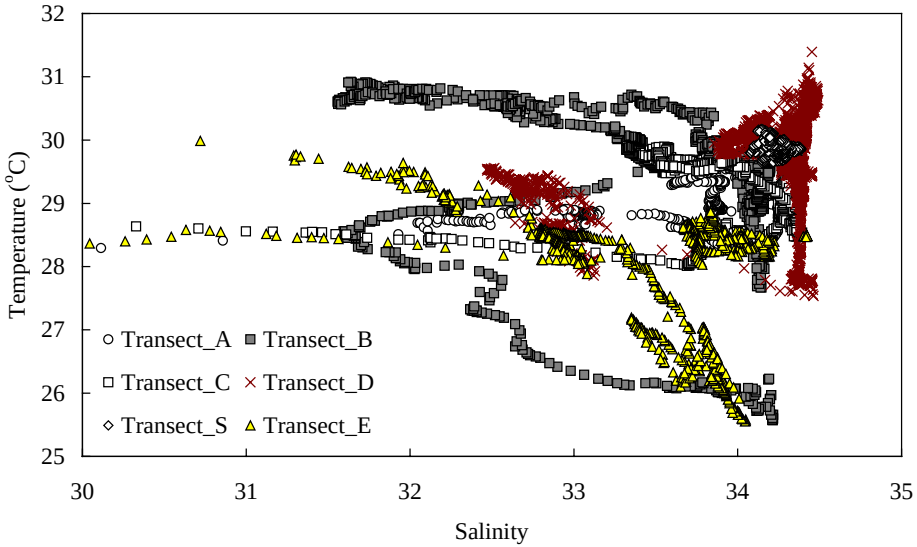

Fig. 3. Surface T-S diagram for salinity >30. Note that in the PRE and the adjacent coastal waters, salinity was <25 along with a temperature of 27–29°C (Fig. 2a).

BGD
6, 6249–6269, 2009

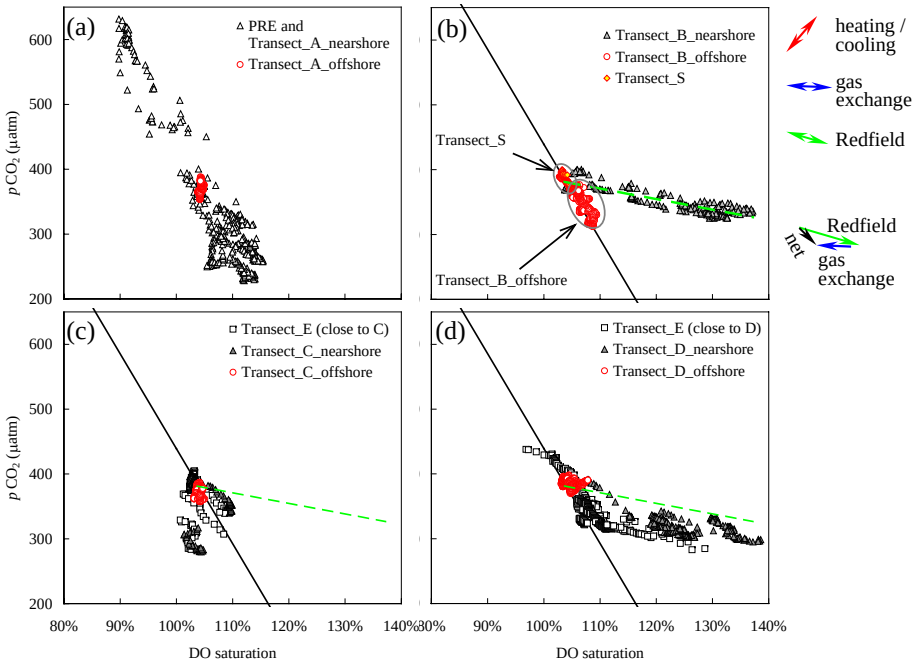

Fig. 4. Relationship between surface pCO_2 and DO saturation along different transects. The two regression lines, fitted by minimizing the sum of the squares of the y-offsets, are: in the nearshore area in Transect B – $y=-164x+552$ ($R^2=0.79$, dashed lines) and the offshore area in Transect B – $y=-1465x+1904$ ($R^2=0.88$, solid lines). Arrows rightward to panel **(b)** depict the expected direction of variations in the sea area off the Pearl River estuary owing to different physical and biological forcings (modified from arrows in Fig. 5b). Note that these arrows are slightly different from DeGrandpre et al. (1997) since their data were obtained at the 20-m depth rather than at ocean surface as did in this study.

BGD
6, 6249–6269, 2009

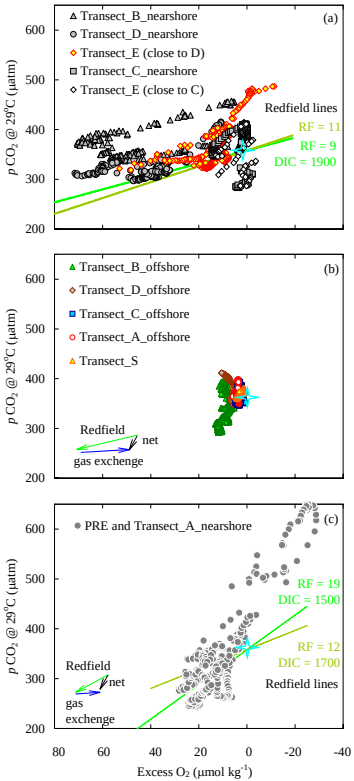

Fig. 5. Temperature normalized pCO_2 (pCO_2 @29°C) vs. excess O_2. The cross star shows the mean atmospheric pCO_2 and the zero excess O_2. In panel **(a)**, the two solid lines show Redfield behavior of pCO_2 @29°C vs. excess O_2 at different Revelle factors (RF) of 9 and 11 in the northern South China Sea (assuming the dissolved inorganic carbon concentration as 1900 µmol kg^{-1}, and ignoring air-sea exchanges). In panel **(c)**, the two solid lines show Redfield behavior of pCO_2 @29°C vs. excess O_2 at different RF in the Pearl River estuary. Arrows depict the expected direction of variations owing to different physical and biological forcings (see text for details).

BGD
6, 6249–6269, 2009